Extended Kalman filter development in Lebesgue sampling framework with an application to Li-ion battery diagnosis and prognosis

Wuzhao Yan[1], and Bin Zhang[2]

[1,2] *Department of Electrical Engineering,*
University of South Carolina, Columbia, SC, 29208, USA
wyan@email.sc.edu
zhangbin@cec.sc.edu

ABSTRACT

Extended Kalman filter in Riemann sampling framework (RS-EKF) has been widely used in diagnosis and prognosis, navigation systems, and GPS for its advantage of simplicity and reasonable solution for nonlinear systems. New particle filter based fault diagnosis and prognosis algorithms in Lebesgue sampling framework have been developed to enable the implementation on systems with limited computational sources, such as embedded systems. In this Lebesgue sampling-based approach, Lebesgue states are defined on the fault dimension axis and algorithm is executed only when the measurement causes a transition from one Lebesgue state to another, or an event happens. This is a need-based fault diagnosis and prognosis (FDP) philosophy in which the algorithm is executed only when necessary, thus less computational resources are required. In order to make algorithms more efficient, EKF algorithm is developed in Lebesgue sampling framework (LS-EKF). With the philosophy of "execution only when necessary", the proposed approach is able to eliminate unnecessary computations, especially in the scenario that the fault grows slowly. The prediction horizon defined by Lebesgue states on the fault dimension axis is usually small and, therefore, LS-EKF naturally benefits the uncertainty management by reducing the uncertainty accumulation. One feature of diagnosis and prognosis in Lebesgue sampling is that it requires two models, one for diagnosis and one for prognosis. The diagnostic model describes the dynamics of fault and is used to estimate the fault state. Prognostic model for LS-EKF describes the time for fault state reaching each defined Lebesgue state. The new algorithms is verified with an application to the diagnosis and prognosis of the state of health of Li-ion battery. The results show that LS-EKF and RS-EKF have comparable performance in diagnosis but LS-EKF has much less computation. Moreover, LS-EKF is more accurate and time-efficient on long term prognosis than RS-EKF algorithms, which makes it a promising solution for FDP in distributed applications.

1. INTRODUCTION

Condition-based maintenance (CBM) and Prognosis and Health Management (PHM), which refers to health monitoring of complex engineering systems based on minimal invasive condition measurements, become active research topics in the past decades. Reliable diagnosis and time-efficient prognosis are important for maintenance and essential for fault detection and remaining useful life (RUL) prediction of critical components, such as batteries, bearings, and drivetrains (Strangas, Aviyente, Neely, & Zaidi, 2013; Orchard, Hevia-Koch, Zhang, & Tang, 2013; Cheng & Pecht, 2009; Capolino & Filippetti, 2013; Immovilli, Bianchini, Cocconcelli, Bellini, & Rubini, 2013; Lou & Loparo, 2004; Bellini, Filippetti, Tassoni, & Capolino, 2008; Zhang et al., 2011). Extended Kalman filter (EKF) is widely used in navigation, mission planning, economic prediction, and state estimation due to the simplicity and capability to handle nonlinear systems (Lall, Lowe, & Goebel, 2011; Lall, Wei, & Goebel, 2012).

With the increasing of system complexity, the utilization of embedded systems grows rapidly. Traditional centralized PHM design cannot meet the demands of carrying more complicated and critical functions to monitor and troubleshoot components for timely and optimal maintenance because of the limitation of communication bandwidth, computational sources, and power consumption. Thus, distributed system design is widely accepted in engineering design, especially for complicated systems (Genc & Lafortune, 2007; Qiu, Wen, & Kumar, 2009; Kumar & Takai, 2009; Liu, Qin, & Chai, 2013; Lefebvre, 2014). With this tendency, more and more FDP algorithms are deployed on local processors and embed-

ded systems to alleviate the requirements on communication bandwidth among the micro-controllers. However, these local processors and embedded systems have limited computational capabilities, which cannot afford the traditional Riemann sapling (RS) based FDP algorithms. RS-based FDP (RS-FDP) takes samples and executes algorithms in periodic time intervals (Olivares, Cerda Munoz, Orchard, & Silva, 2013; Pola et al., 2015; Xian, Long, Li, & Wang, 2014) and, in most cases, requires significant computational resources because of iterative calculations.

To overcome this bottleneck, a novel Lebesgue sampling-based FDP (LS-FDP) framework was developed (Wang & Zhang, 2014; Zhang & Wang, 2014; Yan, Zhang, Wang, Dou, & Wang, 2016), in which FDP algorithms are executed "as-needed". The execution of FDP is triggered only when the value of feature, or condition indicator, changes from one Lebesgue state to another, or an event happens. This event-based diagnosis adopts the philosophy of "execution only when necessary", which significantly reduces the computation requirements by eliminating unnecessary computation. LS-based prognostic algorithm is executed based on the Lebesgue sampling model (LSM) to estimate distributions of operating time for the fault state reaching each Lebesgue state. The prediction horizon of LS-FDP is defined on the fault dimension axis and represented by the number of Lebesgue states. This eliminates the recursive state estimation in RS-based prognosis and provides a straightforward method to conduct prognosis that requires little computational resources.

In our previous works, the LS-FDP was developed with particle filter method, in which the distributions of fault state and RUL are approximated by a set of particles whose dynamics are governed by the diagnostic and prognostic models. From the computation point of view, it is not the optimal method, especially for those systems with small nonlinearities. EKF has much less requirements on computation and has demonstrated performance in many applications. It linearizes the nonlinear system model, and calculates the mean and variance of the system state based on the linearized system model instead of the progress of every particle. In this paper, the Lebesgue sampling and EKF are integrated to design a more efficient LS-EKF algorithm for state estimation and RUL prediction in nonlinear systems. The proposed method takes full advantage of EKF and Lebesgue sampling to reduce computation and make it possible to be deployed on most of the distributed FDP systems.

The paper is organized as follows: Section 2 provides an overview of Lebesgue sampling method and EKF, and the new LS-EKF based on Lebesgue sampling method is developed. A case study based on lithium ion battery is presented to demonstrate the advantages of LS-EKF in Section 3, the experimental results of the EKF competitor are also shown. Conclusions and future research topics are given in Section 4.

2. LEBESGUE SAMPLING-BASED EXTENDED KALMAN FILTER

Kalman filter is a recursive algorithm that estimates the true state of a linear system based on noisy measurements. It assumes that the system can be described by a linear dynamic model and the noise is subject to Gaussian, which is not always true in real applications. Extended Kalman filter (EKF) is developed by linearizing the dynamic model using Taylor expansion at a local point. EKF has been used for prognosis of electronic components and battery management in the Riemann sampling framework (Lall et al., 2012; Saha, Goebel, & Christophersen, 2009). With the new concept of Lebesgue sampling, it is desirable to study the performance and characteristics of FDP with EKF algorithms.

Suppose the fault dynamics can be described by the following nonlinear model:

$$x_k = f(x_{k-1}, u_{k-1}) + \omega_{k-1} \tag{1}$$

where x_k is the states to be estimated, $f(\cdot)$ is the nonlinear function of states, u_k is the input at time k, w_k is a zero mean Gaussian noises with covariance matrix Q_k. Since most faults cannot be measured directly, it relies on some measurable variables. The observation model that describes the relationship between state x_k and measurements z_k is given by:

$$z_k = h(x_k) + v_k \tag{2}$$

where z_k is the measurement, $h(\cdot)$ is the measurement function of state, which can be linear or nonlinear, v_k is a zero-mean Gaussian noises with covariance matrix R_k.

Since $f(\cdot)$ and $h(\cdot)$ are nonlinear functions, they cannot be used to calculate the covariance directly. Instead, their Jacobian are calculated as follows:

$$\begin{aligned} F_k &= \frac{\partial f}{\partial x} \mid_{\hat{x}_{k-1|k-1}} \\ H_k &= \frac{\partial h}{\partial x} \mid_{\hat{x}_{k-1|k-1}} \end{aligned} \tag{3}$$

Note that the Jacobian needs to be calculated with the predicted state at each instant.

The EKF algorithm includes two steps: the first step (prediction) is to propagate the state vector x into the next time step by using the state transition model; the second step (update) is to correct the prediction from the first step by using the

measurement z. The prediction step can be described as:

$$\begin{aligned} \hat{x}_{k|k-1} &= f(\hat{x}_{k-1|k-1}, u_k) \\ P_{k|k-1} &= F_k P_{k|k-1} F_k^T + Q_k \end{aligned} \tag{4}$$

where P_k and Q_k are the covariance matrices of the predicted state and the process noises.

The equations for the update state are expressed as:

$$\begin{aligned} \tilde{y} &= z_k - h(\hat{x}_{k|k-1}) \\ S_k &= H_k P_{k|k-1} H_k^T + R_k \\ K_k &= P_{k|k-1} H_k^T S_k^{-1} \\ P_{k|k} &= (I - K_k H_k) P_{k|k-1} \\ \hat{x}_{k|k} &= \hat{x}_{k|k-1} + K_k \tilde{y}_k \end{aligned} \tag{5}$$

where $\tilde{y}_k$ is the measurement residual, S_k is the residual covariance, K is the near-optimal Kalman gain, R_k is the covariance matrix of the observation noises, $P_{k|k}$ is the updated covariance estimate, $\hat{x}_{k|k}$ is the updated state estimate, and I is the identity matrix.

Lebesgue sampling (LS) is introduced in diagnosis and prognosis by (Wang & Zhang, 2014; Zhang & Wang, 2014). Different from RS method, LS method divides the state axis by a number of predefined states (also called Lebesgue states). The FPD is triggered only when the feature value changes from one Lebesgue state to another, or an event happens. The prediction horizon is described by the number of the Lebesgue states instead of the periodic sampling intervals in RS framework. This LS-based FPD is need-based and its execution is justified by an event. These features enable it to significantly reduce the computation demands and the uncertainty accumulation by eliminating unnecessary computation and decreasing the prediction horizon.

When LS-based prognosis is activated, prognostic algorithm is executed based on the Lebesgue sampling model (LSM) to estimate distributions of operating time for the fault state reaching each Lebesgue state. The LSM is described as:

$$t_{k+1} = t_k + g_t(D(t_k), \hat{x}(t_k), \dot{\hat{x}}(t_k)) + \omega_t(t_k) \tag{6}$$

where t_k is the operation time for fault state reaching the k-th Lebesgue sate, D is the Lebesgue state length, $\omega_t(t_k)$ represents the uncertainties, and $g_t(\cdot)$ is a nonlinear function that describes the time distribution of the fault state arriving at each Lebesgue state. Note that the output of diagnosis at the time instant of the current event t_d is a fault state distribution defined on the state axis, which cannot be used in LS-based prognosis, which is based on Eq. (6) and needs an initial distribution of operation time. To obtain the time distribution on the current Lebesgue state, the time instant of the current event t_d is set to be the mean of the time distribution μ_t, the sigma point $\mu_x - \sigma_x$ of the state distribution has a cross point with the filtered feature curve, which is marked in Figure 1. The coordinates of the cross point $(\mu_t - \sigma_t, \mu_x - \sigma_x)$ represent that sigma point $\mu_x - \sigma_x$ reaches the threshold at time instant $\mu_t - \sigma_t$. The time interval between t_d and the marked point in Figure 1 is set to be the variance of the time distribution. By this method, the variance of state distribution σ_x is approximately converted to that of the time distribution σ_t. Here, μ_x, σ_x, μ_t, and σ_t are the mean and variance of the state estimation, the mean and variance of the time distribution, respectively. The details are shown in Figure 1. For the case of hazard zone, the overlap of state distribution and the hazard zone can be calculated to get a new distribution PDF_h, and it can be converted to a time distribution with the same method mentioned above.

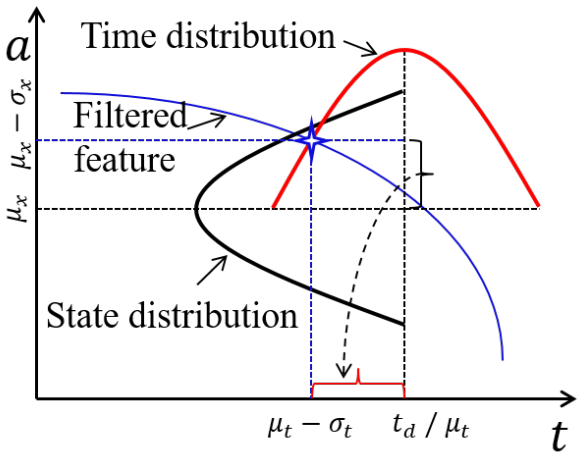

Figure 1. Conversion from state distribution to time distribution

3. AN APPLICATION TO LITHIUM ION BATTERY DIAGNOSIS AND PROGNOSIS

Battery is a safety critical component that provides power for most autonomous systems, such as computers, robots, electrical vehicles, and unmanned aircraft (Pola et al., 2015; Olivares et al., 2013; Zhang, Tang, DeCastro, Roemer, & Goebel, 2014; Scacchioli et al., 2014). Diagnosis and prognosis are critical for estimating the battery state, such as state-of-health (SOH), state-of-charge (SOC), and remaining useful life (RUL) in order to ensure the devices work as expected. In this section, the proposed LS-EKF method is verified in a case study of the diagnosis and prognosis of SOH of lithium ion battery. The results are compared against those from RS-EKF to illustrate the advantages of LS-EKF.

The experiment investigates the SOH of a Li-ion battery with 1.1 Ah rated capacity. The degradation of the capacities is obtained from charge-discharge tests on an Arbin BT2000 battery test system under room temperature at a discharge cur-

rent of 1.1 A (He, Williard, Osterman, & Pecht, 2011). The charge-discharge cycle is cut off at pre-determined cut-off voltages. The failure threshold for the SOH is set as 0.35Ah and the battery capacity reaches this threshold at the 810th cycle.

3.1. EKF in Riemann sampling framework

In traditional Riemann sampling framework, samples are taken equivalently along the time axis. The diagnosis and prognosis model is identically developed and is written as:

$$C(t+1) = C(t) - \gamma \cdot (p_1 + p_2 \cdot t + p_3 \cdot t^2)^{p_4} + \omega_C(t) \quad (7)$$

where C is battery capacity, t is the time index given by cycle number, $p = [0.01, 45, 0.2, 1.25]$ are parameters, γ is a hyper model parameter with mean of $1.6e^{-8}$ and variance of $5e^{-12}$, and ω_C is a model noise.

Figure 2 shows the diagnostic results at the 400th cycle. The mean of capacity estimation is 0.9418 and the 95% confidence interval is [0.939, 0.9446]. The upper sub-figure is the comparison of the capacity from Arbin system against the capacity estimation from EKF. The bottom sub-figure shows the comparison of initial baseline probability distribution function (pdf) (green) compared with the real-time estimated pdf (magenta) at the 400th cycle. Note that the diagnostic algorithm is executed 400 times in the past 400 cycles, *i.e.*, every time when a new measurement becomes available.

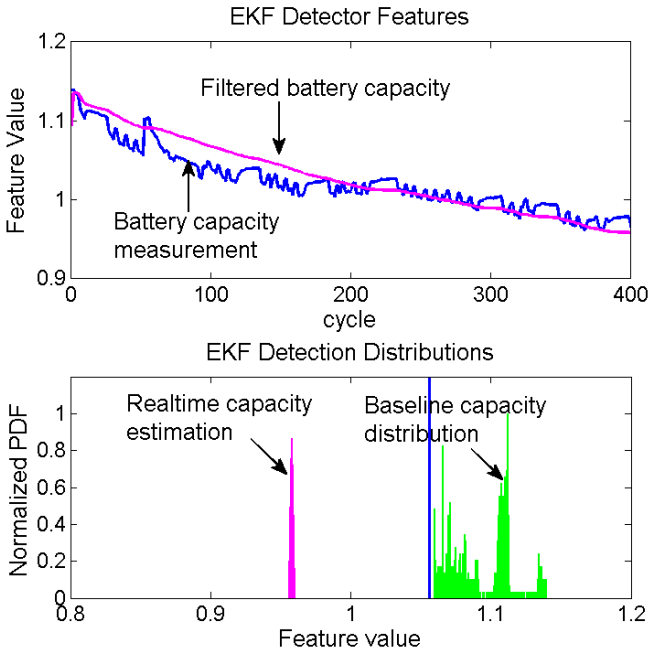

Figure 2. RS-EKF diagnosis for battery at 400th cycle.

With an estimation of the current battery capacity as the initial condition, the prognosis is executed to conduct the long-term prediction and estimation of RUL. Figure 3 shows the expected value, upper and lower bounds of 95% confidence interval (CI) of the battery capacity pdf at each future cycle.

The TTF distribution from EKF-based prognosis is a Gaussian distribution with mean value of 833 cycles when the mean predicted fault size reaches the failure threshold. The upper-bound and lower-bound of the distribution are calculated based on Eq. (4) in EKF algorithm, and can be simply approximated as the time instant when the upper-bound and lower-bound of the capacity distribution reach the failure threshold, details are shown in Figure 1. By this means, the standard deviation of the TTF distribution is approximated to be 59.25 cycles.

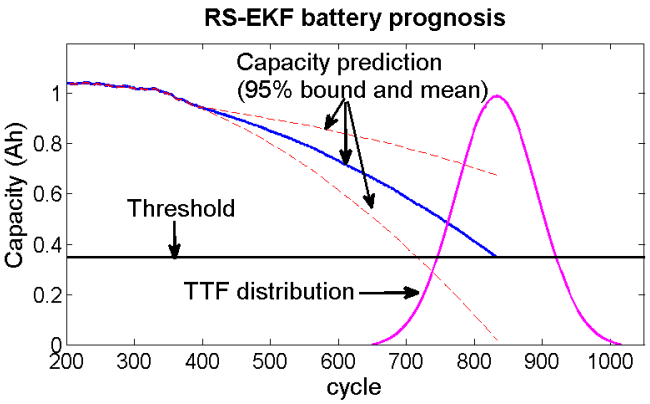

Figure 3. RS-EKF prognosis for battery at 400th cycle.

In this figure, the predicted RUL is 433 cycles. The distance between the prediction and ground truth is 23 cycles. The 95% confidence interval of the RUL pdf is [714.5 951.5], which indicates that the uncertainty accumulated along the prediction horizon is very large.

3.2. EKF in Lebesgue sampling framework

In LS-FDP, the feature value range is divided into a series of Lebesgue states. If a new measurement causes a transition of Lebesgue state, *i.e.*, an event happens, the diagnostic algorithm is executed.

To implement LS-FDP for the battery capacity degradation, initially, 40 uniformly distributed Lebesgue states are defined in the battery's full capacity of 1.1Ah. With this setting, the diagnostic algorithm is executed only when the capacity degrades from one Lebesgue state to another. During the diagnosis process, the length of the Lebesgue states is optimally adjusted according to the fault growth speed. If the fault grows faster, the next Lebesgue length will be decrease, otherwise, the next Lebesgue length will be increased. The adjustment details are illustrated in (Yan, Dou, Liu, Peng, &

Zhang, 2015). The number of Lebesgue states changes during this optimization process.

The model for diagnosis is given by:

$$C(t_{k+1}) = C(t_k) - p_d \cdot C(t_k) \cdot D \cdot sgn(C(t_k) - C(t_{k-1})) + \omega_C(t_k) \quad (8)$$

where t_k is the time instant of the k-th event, p_d is a constant, D is the Lebesgue length, which is given by the difference between two successive Lebesgue states, $\omega_C(t_k)$ is the noise term.

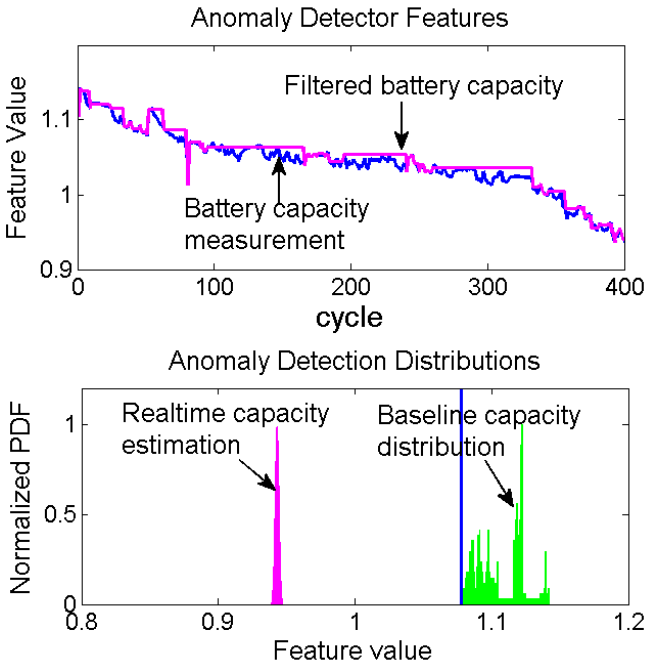

Figure 4. LS-EKF diagnosis for battery at 400th cycle.

Figure 4 shows the diagnostic results at the 400th cycle based on LS-EKF. The mean of capacity estimation is 0.9407 and the 95% confidence interval is [0.925, 0.9608]. Same as the example in RS-EKF, the upper sub-figure shows the comparison of capacity from Coulomb counting (blue) against the estimated mean value from diagnosis (magenta). The lower sub-figure shows the comparison of initial baseline pdf compared with the real-time estimated pdf at the 400th cycle. Note that the diagnostic algorithm is only executed 70 times in the past 400 cycles.

The output of fault diagnosis is the fault state distributions at the current time instant, which cannot be used for LS-based prognosis directly and has to be transformed into the operation time distribution. To implement prognosis in LS-EKF framework, the operation time distribution is achieved as discussed in Figure 1, which is used as the initial condition for prognosis.

Prognostic part in LS-EKF is conducted on fault dimension axis to predict the time-to-Lebesgue-state directly. The model for prognosis is given as:

$$t_{k+1} = t_k + p_p \cdot C(t_k) \cdot D \cdot exp\left(-\dot{C}(t_k)\right) + \omega_t(t_k) \quad (9)$$

where p_p is a constant and ω_t is the model noise.

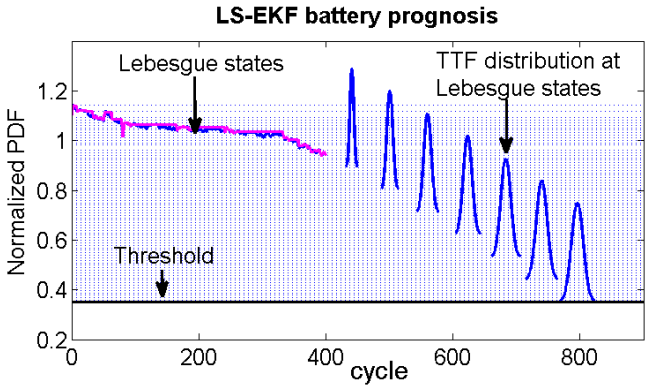

Figure 5. LS-EKF prognosis for battery at 400th cycle.

Figure 5 shows the prognostic results at the 400th cycle. To make the figure clear, only the time distribution pdf at a few selected Lebesgue state are plotted. The prediction horizon is 59 Lebesgue states, which is very small compare to the 433 cycles in RS-EKF. The predicted TTF for this battery is 795.7 and the RUL is 395.7 cycles. The 95% confidence interval of the TTF distribution is [786.7 804.7]. The uncertainty is much smaller than that of RS-based prognosis due to the small prediction horizon. Compared with the ground truth TTF of 810,the difference between ground truth and the prediction is 14.3 cycles.

3.3. Comparison of RS-EKF and LS-EKF

Compared to RS-EKF prognosis with large horizon (433 cycles), the LS-EKF prognosis shown in Figure 5 only has a prognostic horizon of 59 Lebesgue states. The reduction of computation time is (0.055146-0.007064)/0.055146=87.19% and the computation is about 7.8 times faster.

Diagnostic and prognostic results of RS-EKF and LS-EKF algorithms are compared in Table 1. Compared with RS-EKF prognosis with a horizon of 433 cycles at the 400th cycle, the LS-EKF prognosis has a horizon of 59 Lebesgue states. The computation time for every LS-EKF prognosis routine is only 12.8% of that of the RS-EKF prognosis. Note that the Lebesgue state length in the LS-EKF prognosis is changed according to the fault growth speed to keep a closer monitoring on the SOH. If the fault growth speed becomes faster along the prediction steps, the Lebesgue state length for the following prediction steps will be decreased, otherwise, it will be increased. The computational sources is optimally distributed during the diagnosis and prognosis process by increasing the

Lebesgue state length and reducing the unnecessary execution when the fault grows slowly. When the fault grows fast, more computational sources is assigned to the FDP algorithm to monitor the health state of the system.

Diagnosis results	RS-EKF	LS-EKF
Capacity expectation	0.9418	0.9406
Capacity 95% CI	[0.939 0.9446]	[0.9205 0.9607]
Execution numbers	400 (100%)	70 (17.5%)
Prognosis results	RS-EKF	LS-EKF
True TTF	810	810
Estimate TTF	833	795.7
95% CI of TTF	[714.5 951.5]	[786.7 804.7]
Prognostic horizon	433	59
Computation time	0.55146 (100%)	0.007064 (12.8%)

Table 1. Comparison of Traditional RS-EKF and LS-EKF for Battery

Accuracy is one of the most important properties in FDP. In order to compare the accuracy of RS-EKF and LS-EKF methods, α - λ matrix is introduces in (Saxena, Celaya, Saha, Saha, & Goebel, 2010), as shown in Figure 6 with $\alpha = 0.3$. The matrix is defined as:

$$[1-\alpha]\cdot r_t(t_k) \leq r^l(t_k) \leq [1+\alpha]\cdot r_t(t_k) \qquad (10)$$

where r^l is the predicted RUL at the lth time instant, r_t is the ground truth TTF, α is the accuracy modifier (Saxena et al., 2010).

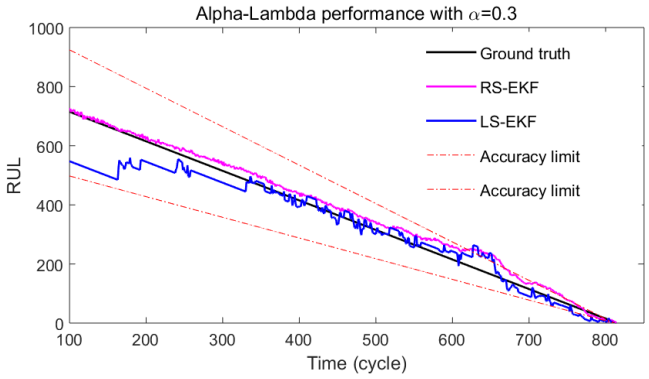

Figure 6. Prediction accuracy comparison between RS-EKF and LS-EKF.

Judging from Figure 6, the mean of the predicted RUL for RS-EKF is as accurate as that of LS-EKF. However, the variance of predicted RUL of LS-EKF is much smaller as shown in Table 1, which is the natural benefit from Lebesgue sampling methodology, since the prediction horizon in LS-EKF is much smaller than that of RS-EKF, the uncertainty accumulation during the prediction process is much smaller. Based on these advantages, LS-EKF can provide strong support for decision-making. More importantly, the LS-EKF required less calculation sources compared with RS-EKF, which makes it more feasible for distributed FDP with limited computational sources.

4. CONCLUSION

EKF based diagnosis and prognosis methods were developed based on Riemann sampling framework with great achievement for its simplicity. With the trend of distributed FDP, Lebesgue sampling method is introduced with a philosophy of "execution when needed" to reduce the computation and make the long-term online prognosis possible on embedded systems. In this paper, EKF algorithm is developed in the Lebesgue sampling framework. An experiment of Lithium-ion battery SOH diagnosis and prognosis with comparison against traditional RS-based approach is presented. It is demonstrated that the proposed approach is able to reduce the requirement on computational sources compared with traditional RS-EKF. This proposed approach combines the advantages of EKF and LS method, which results in low computation and small uncertainty accumulation.

REFERENCES

Bellini, A., Filippetti, F., Tassoni, C., & Capolino, G. A. (2008, Dec). Advances in diagnostic techniques for induction machines. *IEEE Transactions on Industrial Electronics*, *55*(12), 4109-4126. doi: 10.1109/TIE.2008.2007527

Capolino, G.-A., & Filippetti, F. (2013). Introduction to the special section on advances in diagnosis for electrical machines, power electronics, and drives-part i. *Industrial Electronics, IEEE Transactions on*, *60*(8), 3396–3397.

Cheng, S., & Pecht, M. (2009). A fusion prognostics method for remaining useful life prediction of electronic products. In *Automation science and engineering, 2009. case 2009. ieee international conference on* (pp. 102–107).

Genc, S., & Lafortune, S. (2007, April). Distributed diagnosis of place-bordered petri nets. *Automation Science and Engineering, IEEE Transactions on*, *4*(2), 206-219. doi: 10.1109/TASE.2006.879916

He, W., Williard, N., Osterman, M., & Pecht, M. (2011). Prognostics of lithium-ion batteries based on dempster–shafer theory and the bayesian monte carlo method. *Journal of Power Sources*, *196*(23), 10314–10321.

Immovilli, F., Bianchini, C., Cocconcelli, M., Bellini, A., & Rubini, R. (2013). Bearing fault model for induction motor with externally induced vibration. *Industrial Electronics, IEEE Transactions on*, *60*(8), 3408–3418.

Kumar, R., & Takai, S. (2009, July). Inference-based ambiguity management in decentralized decision-making: Decentralized diagnosis of discrete-event systems. *Au-*

tomation Science and Engineering, IEEE Transactions on, *6*(3), 479-491. doi: 10.1109/TASE.2009.2021330

Lall, P., Lowe, R., & Goebel, K. (2011, June). Extended kalman filter models and resistance spectroscopy for prognostication and health monitoring of leadfree electronics under vibration. In *Prognostics and health management (phm), 2011 ieee conference on* (p. 1-12). doi: 10.1109/ICPHM.2011.6024324

Lall, P., Wei, J., & Goebel, K. (2012). Comparison of kalman-filter and extended kalman-filter for prognostics health management of electronics. In *Thermal and thermomechanical phenomena in electronic systems (itherm), 2012 13th ieee intersociety conference on* (pp. 1281–1291).

Lefebvre, D. (2014, Oct). Fault diagnosis and prognosis with partially observed petri nets. *Systems, Man, and Cybernetics: Systems, IEEE Transactions on*, *44*(10), 1413-1424. doi: 10.1109/TSMC.2014.2311760

Liu, Q., Qin, S., & Chai, T. (2013, July). Decentralized fault diagnosis of continuous annealing processes based on multilevel pca. *Automation Science and Engineering, IEEE Transactions on*, *10*(3), 687-698. doi: 10.1109/TASE.2012.2230628

Lou, X., & Loparo, K. A. (2004). Bearing fault diagnosis based on wavelet transform and fuzzy inference. *Mechanical systems and signal processing*, *18*(5), 1077–1095.

Olivares, B., Cerda Munoz, M., Orchard, M., & Silva, J. (2013, Feb). Particle-filtering-based prognosis framework for energy storage devices with a statistical characterization of state-of-health regeneration phenomena. *Instrumentation and Measurement, IEEE Transactions on*, *62*(2), 364-376. doi: 10.1109/TIM.2012.2215142

Orchard, M. E., Hevia-Koch, P., Zhang, B., & Tang, L. (2013). Risk measures for particle-filtering-based state-of-charge prognosis in lithium-ion batteries. *Industrial Electronics, IEEE Transactions on*, *60*(11), 5260–5269.

Pola, D., Navarrete, H., Orchard, M., Rabie, R., Cerda, M., Olivares, B., ... Perez, A. (2015, June). Particle-filtering-based discharge time prognosis for lithium-ion batteries with a statistical characterization of use profiles. *Reliability, IEEE Transactions on*, *64*(2), 710-720. doi: 10.1109/TR.2014.2385069

Qiu, W., Wen, Q., & Kumar, R. (2009, April). Decentralized diagnosis of event-driven systems for safely reacting to failures. *Automation Science and Engineering, IEEE Transactions on*, *6*(2), 362-366. doi: 10.1109/TASE.2008.2009093

Saha, B., Goebel, K., & Christophersen, J. (2009). Comparison of prognostic algorithms for estimating remaining useful life of batteries. *Transactions of the Institute of Measurement and Control*.

Saxena, A., Celaya, J., Saha, B., Saha, S., & Goebel, K. (2010). Metrics for offline evaluation of prognostic performance. *International Journal of Prognostics and Health Management*, *1*(1), 20.

Scacchioli, A., Rizzoni, G., Salman, M., Li, W., Onori, S., & Zhang, X. (2014, Jan). Model-based diagnosis of an automotive electric power generation and storage system. *Systems, Man, and Cybernetics: Systems, IEEE Transactions on*, *44*(1), 72-85. doi: 10.1109/TSMCC.2012.2235951

Strangas, E. G., Aviyente, S., Neely, J. D., & Zaidi, S. S. H. (2013). The effect of failure prognosis and mitigation on the reliability of permanent-magnet ac motor drives. *Industrial Electronics, IEEE Transactions on*, *60*(8), 3519–3528.

Wang, X., & Zhang, B. (2014, Dec). Real-time lebesgue-sampled model for continuous-time nonlinear systems. In *Decision and control (cdc), 2014 ieee 53rd annual conference on* (p. 4367-4372). doi: 10.1109/CDC.2014.7040070

Xian, W., Long, B., Li, M., & Wang, H. (2014, Jan). Prognostics of lithium-ion batteries based on the verhulst model, particle swarm optimization and particle filter. *Instrumentation and Measurement, IEEE Transactions on*, *63*(1), 2-17. doi: 10.1109/TIM.2013.2276473

Yan, W., Dou, W., Liu, D., Peng, Y., & Zhang, B. (2015). Parameters adaption of lebesgue sampling-based diagnosis and prognosis for li-ion batteries. In *Annual conference of the prognostics and health management society 2015* (Vol. 6).

Yan, W., Zhang, B., Wang, X., Dou, W., & Wang, J. (2016, March). Lebesgue-sampling-based diagnosis and prognosis for lithium-ion batteries. *IEEE Transactions on Industrial Electronics*, *63*(3), 1804-1812. doi: 10.1109/TIE.2015.2494529

Zhang, B., Sconyers, C., Byington, C., Patrick, R., Orchard, M., & Vachtsevanos, G. (2011, May). A probabilistic fault detection approach: Application to bearing fault detection. *Industrial Electronics, IEEE Transactions on*, *58*(5), 2011-2018. doi: 10.1109/TIE.2010.2058072

Zhang, B., Tang, L., DeCastro, J., Roemer, M., & Goebel, K. (2014). Autonomous vehicle battery state-of-charge prognostics enhanced mission planning. *Int. J. Prognost. Health Manage*, *5*(2), 1–12.

Zhang, B., & Wang, X. (2014). Fault diagnosis and prognosis based on lebesgue sampling. In *Annual conference of the prognostics and health management society 2014* (Vol. 5).